Eur. Phys. J. D **26**, 51–57 (2003)
DOI: 10.1140/epjd/e2003-00082-0

THE EUROPEAN PHYSICAL JOURNAL D

Dissociative ionization of molecules in intense laser fields

D. Dundas[a], K.J. Meharg, J.F. McCann, and K.T. Taylor

Department of Applied Mathematics and Theoretical Physics, Queen's University Belfast, University Road, Belfast BT7 1NN, Northern Ireland, UK

Received 19 November 2002
Published online 24 April 2003

Abstract. Accurate and efficient grid based techniques for the solution of the time-dependent Schrödinger equation for few-electron diatomic molecules irradiated by intense, ultrashort laser pulses are described. These are based on hybrid finite-difference, Lagrange mesh techniques. The methods are applied in three scenarios, namely H_2^+ with fixed internuclear separation, H_2^+ with vibrating nuclei and H_2 with fixed internuclear separation and illustrative results presented.

PACS. 02.60.Cb Numerical simulation; solution of equations – 02.70.Bf Finite-difference methods – 33.80.Rv Multiphoton ionization and excitation to highly excited states (e.g., Rydberg states) – 33.80.-b Photon interactions with molecules

1 Introduction

The interaction of few-electron diatomic molecules with intense, ultrashort laser pulses is of fundamental importance in femtosecond chemistry. Such systems allow us to study the interplay between electron dynamics and nuclear dynamics and as such act as a precursor to the description of more complex molecular systems. From a physical point of view these systems are also of fundamental importance since they provide examples of quantum systems driven far from equilibrium and thus allow us to study highly non-linear phenomena, such as ionization (multiphoton, tunnelling and above-threshold), high-order harmonic generation, dissociation and Coulomb explosions [1–4].

The simplest few-electron diatomic molecules are the one-electron hydrogen molecular ion (H_2^+) and the two-electron hydrogen molecule (H_2) which have been the basis of much study, both experimentally and theoretically. Most experimental studies have to date focussed on H_2 [1] due to the relative ease of preparing neutral beams. In the last few years, however, experimental techniques have advanced to the point where H_2^+ can be studied using ion beam techniques [5,6]. Theory, on the other hand has concentrated primarily on H_2^+ [7–10] due to the relative ease of performing such calculations, indeed it has only been in the last few years that attention has seriously focussed on H_2 [11–13].

In this paper we set out our method for treating both of these systems. The testing bed for our approaches has been H_2^+ where we first consider a fixed internuclear separation, subsequently removing this constraint. For the laser pulses considered in this work, pulse duration are sufficiently short enough so that nuclear rotation effects are negligible and we have taken the internuclear axis aligned to the laser polarization axis. These two systems allow us to develop approaches firstly for the electron dynamics and secondly for the nuclear dynamics which are then taken over to model H_2 with a fixed internuclear separation. The paper is arranged as follows. Section 2 details the theoretical description of the three problems. In Section 3 the grid methods used in the solution of the problems are briefly discussed. Section 4 presents some illustrative results for each problem and Section 5 draws some conclusions. Atomic units are used throughout.

2 Theoretical treatment

An accurate theoretical description of laser-driven diatomic molecules requires the solution of the time-dependent Schrödinger equation (TDSE)

$$H\Psi = \mathrm{i}\frac{\partial}{\partial t}\Psi, \tag{1}$$

where H is the time-dependent Hamiltonian and Ψ the wavefunction. For a linearly-polarized laser pulse with the internuclear axis aligned along the polarization axis, cylindrical polar coordinates are the most natural choice with the electron position vector given by

$$\mathbf{r} = \rho\cos\phi\mathbf{i} + \rho\sin\phi\mathbf{j} + z\mathbf{k}, \tag{2}$$

where the axial coordinate (z) is along the polarization direction. The z coordinate is therefore predominant since most electron motion will be driven along the axis of polarization. The radial (ρ) coordinate of each electron,

[a] e-mail: d.dundas@qub.ac.uk

while less important, are still required for a proper description of the exchange of angular momentum between the electrons and the field. With the chosen alignment of the molecule a cylindrical symmetry exists about the internuclear axis which greatly simplifies the handling of both H_2^+ and H_2. For instance for H_2^+ the single electron wavefunction will have no ϕ dependence. Thus the fixed-nuclei problem involves in this case merely the solution of a (2+1)-dimensional TDSE whilst allowing the nuclei to move along the polarization axis requires the solution of a (3+1)-dimensional TDSE. For H_2 symmetry also reduces the number of degrees of freedom by one and so H_2 with fixed internuclear spacing demands the solution of a (5+1)-dimensional TDSE. We now set out the Hamiltonian and wavefunction form taken for each of the three problems considered.

2.1 Fixed-nuclei H_2^+

For Σ-symmetry, the azimuthal (ϕ) dependence does not arise and the Hamiltonian has the form

$$H = -\frac{1}{2}\left(\frac{\partial^2}{\partial z^2} + \frac{1}{\rho}\frac{\partial}{\partial \rho}\rho\frac{\partial}{\partial \rho}\right) + V(\rho, z, R) + \frac{Z_1 Z_2}{R} + fU(z,t), \quad (3)$$

where $V(\rho, z, R)$ represents the Coulomb interactions

$$V(\rho, z, R) = -\frac{Z_1}{\sqrt{\rho^2 + \left(z - \frac{1}{2}R\right)^2}} - \frac{Z_2}{\sqrt{\rho^2 + \left(z + \frac{1}{2}R\right)^2}}, \quad (4)$$

R being the internuclear distance and Z_1 and Z_2 the nuclear charges; $fU(z,t)$ represents the interaction between the electron and the laser field. A length gauge description of the electron-field interaction is used in which $U(z,t) = zE(t)$ where $E(t)$ is the electric field strength. For the case of fixed nuclei $f = 1$.

One can remove the first-order derivative in equation (3) by a change of dependent variable

$$\Psi(\rho, z, t) = \frac{1}{\sqrt{2\pi\rho}}\psi(\rho, z, t), \quad (5)$$

such that

$$\mathrm{i}\frac{\partial}{\partial t}\psi(\rho, z, t) = \left[-\frac{1}{2}\left(\frac{\partial^2}{\partial z^2} + D_\rho\right) + V(\rho, z, R) + \frac{Z_1 Z_2}{R} + fU(z,t)\right]\psi(\rho, z, t), \quad (6)$$

where

$$D_\rho = \left(\frac{\partial^2}{\partial \rho^2} + \frac{1}{4\rho^2}\right). \quad (7)$$

In this case wavefunction normalization requires

$$\int_0^\infty \mathrm{d}\rho \int_{-\infty}^{+\infty} \mathrm{d}z\ |\psi(\rho, z, t)|^2 = 1. \quad (8)$$

We then construct a 2D-grid in the ρ and z coordinates and discretize the wavefunction on this grid.

2.2 Vibrating-nuclei H_2^+

Progressing from fixed-nuclei to vibrating-nuclei the wavefunction gains an extra degree of freedom, *i.e.* the internuclear coordinate, and so the propagated wavefunction will be $\psi(R, \rho, z, t)$. The Hamiltonian has the form

$$H = -\frac{1}{M}\frac{\partial^2}{\partial R^2} - \frac{1}{2\mu}\left(\frac{\partial^2}{\partial z^2} + D_\rho\right) + V(\rho, z, R) + \frac{Z_1 Z_2}{R} + fU(z,t). \quad (9)$$

In this case

$$f = 1 + \frac{m_\mathrm{e}}{2M + m_\mathrm{e}}, \quad (10)$$

where M is the mass of each nucleus, m_e is the mass of the electron and μ its reduced mass.

2.3 Fixed-nuclei H_2

In cylindrical coordinates the position vectors of the two electrons are given by

$$\mathbf{r}_s = \rho_s \cos\phi_s \mathbf{i} + \rho_s \sin\phi_s \mathbf{j} + z_s \mathbf{k} \qquad s = 1, 2. \quad (11)$$

The cylindrical symmetry in the problem requires that the wavefunction does not depend on the azimuthal coordinates individually but only the difference between them. In consequence the wavefunction depends on 5 spatial degrees of freedom, namely ρ_1, ρ_2, z_1, z_2, and $\phi = \phi_1 - \phi_2$. By taking into account rotation and reflection symmetries in the wavefunction, we are able to reduce the range of ϕ from $[0, 4\pi]$ to $[0, \pi]$. Taking this reduced range into account, and noting that the wavefunction remains spatially symmetric throughout the laser interaction time, allows us to obtain the relation

$$\Psi(\rho_1, \rho_2, z_1, z_2, \phi, t) = \Psi(\rho_2, \rho_1, z_2, z_1, \phi, t). \quad (12)$$

As in the case of H_2^+ first-order derivatives in the Hamiltonian can be removed by writing

$$\Psi(\rho_1, \rho_2, z_1, z_2, \phi, t) = \frac{1}{\sqrt{4\pi\rho_1\rho_2}}\psi(\rho_1, \rho_2, z_1, z_2, \phi, t), \quad (13)$$

so that

$$\int_0^\pi \mathrm{d}\phi \int_0^\infty \mathrm{d}\rho_1 \int_0^\infty \mathrm{d}\rho_2 \int_{-\infty}^{+\infty} \mathrm{d}z_1 \int_{-\infty}^{+\infty} \mathrm{d}z_2\ |\psi|^2 = 1. \quad (14)$$

The Hamiltonian for the laser-driven H_2 molecule is then of the form

$$H = \sum_{s=1}^{2}\left[-\frac{1}{2}\left\{\frac{\partial^2}{\partial z_s^2} + D_{\rho_s} + \frac{1}{\rho_s^2}\frac{\partial^2}{\partial \phi^2}\right\} + V(\rho_s, z_s, R) + fU(z_s, t)\right] + V_{\mathrm{ee}}(\mathbf{r}_1, \mathbf{r}_2) + \frac{Z_1 Z_2}{R}, \quad (15)$$

where $V_{\rm ee}(\mathbf{r}_1, \mathbf{r}_2)$ represents the electron-electron interaction

$$V_{\rm ee}(\mathbf{r}_1, \mathbf{r}_2) = \frac{1}{\sqrt{\rho_1^2 + \rho_2^2 + (z_1 - z_2)^2 - 2\rho_1\rho_2\cos\phi}}. \quad (16)$$

In this case we construct a 5D spatial grid and discretize the wavefunction on it.

3 Grid techniques

Accurately treating the H_2^+ and H_2 problems necessitates the grid treatment of 4 distinct coordinates, namely ρ, z, ϕ and R. The grid methods employed have to meet various criteria, in order to be not only accurate but efficient. Extending the discussions in [14], we see that each of these grids must fulfill the following criteria:

1. provide adequate coverage of configuration space;
2. allow the correct application of the boundary conditions at $\rho_s = 0$, $s = 1, 2$;
3. allow the correct application of the boundary conditions when $\mathbf{r}_1 = \mathbf{r}_2$;
4. make possible a unitary time evolution operator;
5. provide a large density of grid points along the z_1 and z_2 directions, since electronic motion has largest velocity components parallel to the z-axis (laser polarization axis);
6. provide comparatively fewer grid points along the ρ_1, ρ_2 and ϕ directions;
7. accurately treat the R coordinate.

A Lagrange mesh treatment of the ρ_1, ρ_2 and ϕ and R variables, together with a finite difference treatment of the z_1 and z_2 variables, satisfy these requirements. For an extensive discussion of the relationship between these two approaches the reader is referred to [15]. We now outline the grid methods for each of the four distinct coordinates.

3.1 Lagrange mesh treatment of ρ

The Lagrange mesh method is a basis set method founded on Lagrange interpolation and Gaussian quadrature. It is a special case of the Discrete Variable Representation method [16] which has been extensively applied to both time-independent problems [17,18] and time-dependent problems [19,20]. For a fuller description of the method, the reader is referred to Baye and Heenan [21]. The reader is also referred to [14] for a fuller description of the application of the method to the present problems.

In treating the ρ coordinates we use a mesh having N_ρ quadrature points. These quadrature points are the zeros of the generalized Laguerre polynomials, $L^\alpha_{N_\rho}(\rho)$, where,

$$L^\alpha_{N_\rho}(\rho) = \frac{(\alpha + N_\rho)!}{\alpha! N_\rho!} {}_1F_1(-N_\rho; \alpha + 1; \rho), \quad (17)$$

and are defined over the interval $[0, \infty)$. These quadrature points are denoted by ρ_i, for $i = 1, \ldots, N_\rho$.

Normalized Lagrange functions, $g_i(\rho)$, $i = 1 \ldots, N_\rho$, are obtained through use of the orthonormal set, $\varphi_k(\rho)$, $k = 0 \ldots, N_\rho - 1$, where,

$$\varphi_k(\rho) = \left[\frac{\Gamma(\alpha + k + 1)}{k!}\right]^{-1/2} \rho^{\alpha/2} \mathrm{e}^{-\rho/2} L^\alpha_k(\rho), \quad (18)$$

and have been found to take the form

$$g_i(\rho) = \lambda_i^{-1/2} \frac{1}{\varphi'_{N_\rho}(\rho_i)} \frac{\varphi_{N_\rho}(\rho)}{\rho - \rho_i}, \quad (19)$$

where the quadrature weights are given by

$$\lambda_i = \frac{1}{\rho_i \varphi'_{N_\rho}(\rho_i)^2} \qquad i = 1, \ldots, N_\rho. \quad (20)$$

Using these three sets of variables, it is then possible to evaluate the matrix elements of the ρ-dependent kinetic energy terms $-1/2 D_\rho$ exactly, by setting $\alpha = 1$, so that for $i, j = 1, \ldots, N_\rho$,

$$D_{ij} = -\frac{1}{2} \int_0^\infty g_i^\star(\rho) D_\rho g_j(\rho) \mathrm{d}\rho. \quad (21)$$

Baye and Heenen [21] have shown that the matrix elements are given by

$$D_{ij} = \frac{1}{2} \times \begin{cases} \dfrac{1}{\rho_i^2} + S_{ii} & i = j \\ (-1)^{i-j} \left[\dfrac{1}{\sqrt{\rho_i \rho_j}} \left(\dfrac{1}{\rho_i} + \dfrac{1}{\rho_j}\right) + S_{ij}\right] & i \neq j \end{cases} \quad (22)$$

where

$$S_{ij} = \sqrt{\rho_i \rho_j} \sum_{k \neq i,j} \frac{1}{\rho_k (\rho_k - \rho_i)(\rho_k - \rho_j)}. \quad (23)$$

3.2 Lagrange mesh treatment of R

Treating the internuclear coordinate for vibrating nuclei requires us to evaluate the nuclear kinetic energy term. This coordinate can also be treated with a set of normalized Lagrange functions $h_i(R), i = 1, \ldots N_R$ formed from a Laguerre basis set, $\varphi_k(R)$, $k = 0 \ldots, N_R - 1$, where

$$\varphi_k(R) = \left[\frac{\Gamma(\alpha + k + 1)}{k!}\right]^{-1/2} R^{\alpha/2} \mathrm{e}^{-R/2} L^\alpha_k(R). \quad (24)$$

In this case we choose $\alpha = 0$. Denoting the quadrature points by R_i the matrix elements of the nuclear kinetic energy term are given by

$$T_{ij} = -\frac{1}{M} \int_0^\infty h_i^\star(R) \frac{\partial}{\partial R} h_j(R) \mathrm{d}R \quad (25)$$

Again, Baye and Heenen [21] have shown that the matrix elements are given by

$$T_{ij} = -\frac{1}{M} \times \begin{cases} \dfrac{1}{4R_i^2} + S_{ii} & i = j \\ (-1)^{i-j}\left[\dfrac{1}{\sqrt{2R_iR_j}}\left(\dfrac{1}{R_i}+\dfrac{1}{R_j}\right) + S_{ij}\right] & i \neq j \end{cases} \quad (26)$$

with

$$S_{ij} = \sqrt{R_iR_j}\sum_{k\neq i,j}\frac{1}{R_k(R_k-R_i)(R_k-R_j)}. \quad (27)$$

3.3 Lagrange mesh treatment of ϕ

In the case of the ϕ variable, we seek a set of normalized Lagrange functions and weights, denoted $v_m(\phi)$ and w_m, $m = 1, \ldots, N_\phi$ respectively, defined on the interval $[0, \pi]$, together with a set of quadrature points that would enable us to evaluate the ϕ-dependent kinetic energy terms

$$P_{mn} = \int_0^\pi v_m^\star(\phi)\frac{\partial^2}{\partial\phi^2}v_n(\phi)\,\mathrm{d}\phi \quad (28)$$

exactly.

Karabulut [22] has found such a desirable set, to within a scale factor. Following this work, we choose quadrature points

$$\phi_m = \frac{(2m-1)}{2N_\phi}\pi \qquad m = 1, \ldots, N_\phi, \quad (29)$$

together with normalized Lagrange functions

$$v_m(\phi) = \frac{1}{\sqrt{\pi N_\phi}}\left[1 + 2\sum_{k=1}^{N_\phi-1}\cos(k\phi_m)\cos(k\phi)\right], \quad (30)$$

and quadrature weights

$$w_m = \frac{\pi}{N_\phi} \qquad m = 1, \ldots, N_\phi, \quad (31)$$

giving

$$P_{mn} = \frac{(-1)^{m-n-1}}{2} \times \begin{cases} \dfrac{1}{\sin^2(m-n)\pi/2N_\phi} - \dfrac{1}{\sin^2(m+n-1)\pi/2N_\phi} & m \neq n \\ N_\phi + \dfrac{(N_\phi-1)(2N_\phi-1)}{3} - \dfrac{1}{\sin^2(2m-1)\pi/2N_\phi} & m = n. \end{cases} \quad (32)$$

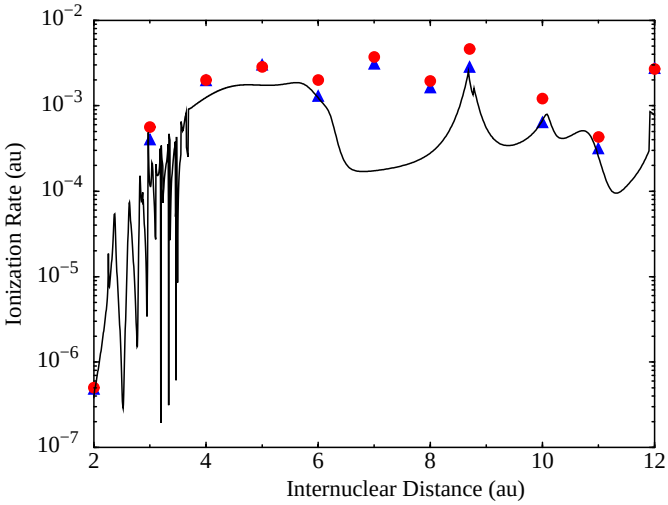

Fig. 1. Comparison of the Lagrange mesh results (▲) for the ionization rate as a function of internuclear separation for a laser pulse of wavelength 248 nm and peak intensity 1.0×10^{14} Wcm^{-2} with the results of Madsen and Plummer [25] (——) and with the finite difference method [10] (•).

3.4 Finite difference treatment of z

As in [10] the z coordinate is treated using finite differences, the kinetic energy term is approximated by the 5-point central difference formula. While higher-order finite difference methods have been used in the past to solve the time-dependent Schrödinger equation for model molecular potentials [23,24], the finite difference approach employed here allows us to parallelize our computer codes efficiently by distributing the z coordinate grid across processors. In order to handle the electron quiver motion in intense and low frequency fields a large number of z grid points must be used. Distributing the z coordinate across processors allows us to scale the size of the problem easily to handle such fields. The sparse nature of the finite difference matrices compared to the Lagrange mesh method means that communications between processors is kept to a minimum. Indeed each processor must communicate with a maximum of two neighbouring processors for H_2^+ and a maximum of four neighbouring processors for H_2.

4 Results

4.1 Fixed nuclei H_2^+ results

In Figure 1 we present a comparison of the ionization rates as a function of internuclear separation for a laser pulse of wavelength 248nm and peak intensity $I_0 = 1.0 \times 10^{14}$ Wcm^{-2} with the results of Madsen and Plummer [25] and with a full finite difference method [10]. A grid having extent $-50 \leq z \leq 50$ and $0 \leq \rho \leq 42$ Bohr was used. The Keldysh parameter for these conditions varies between $\gamma \approx 5$ for $R = 2$ and $\gamma \approx 3$ for large R and this defines the process as multiphoton rather than

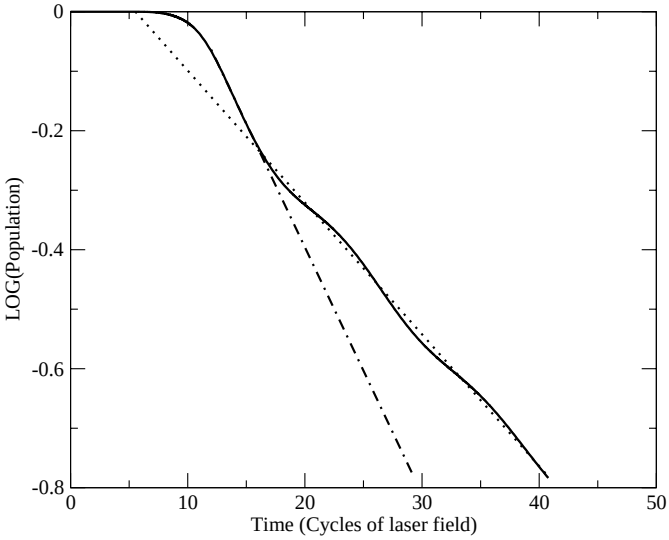

Fig. 2. Logarithm of the electronic population within the grid (——) at $R = 10$ for a wavelength of $\lambda = 248$ nm using and a peak intensity of 1.0×10^{14} Wcm^{-2}. Two distinct rates are present which are highlighted by the extrapolated lines, namely initial population of a bound resonant state (— · —) followed by its subsequent decay (· · · · · ·).

tunneling ionization. Very good agreement between both time-dependent methods is observed for all internuclear distances. Very good agreement with the Floquet results is also found at the equilibrium bond length, $R = 2$, at which the ground electronic state is an isolated resonance of the system requiring six photons to reach the ionization threshold, and at larger internuclear distances where the process requires only four photons to achieve ionization. Poor agreement with the Floquet results is observed around intermediate internuclear distances ($6 < R < 9$). The Floquet ionization rates refer to a particular dressed state formed from the Σ_g^+ ground-state. However, around intermediate values of R the ground state ionization rate is difficult to define. As a result of crossings with excited states and Rydberg series resonances the ground-state becomes mixed (dressed) with other states. Both wavepacket calculations indicate the non-adiabatic following that arises during the pulse rise and indicates the difficulty in comparing with Floquet theory for interfering resonance states.

In obtaining these results we found that the use of a 20 cycle laser pulse having a 4 cycle ramp-on and a 4 cycle ramp-off gave fully converged results except at $R = 8.7$ and $R = 10$. From the figure we see that the Floquet rate is peaked around these values which suggests the presence of an intermediate resonance state. We find that using a 60 cycle laser pulse having a 10 cycle ramp on and a 10 cycle ramp off reproduces the Floquet rate. The reason for this is obvious from Figure 2. In this figure we plot the logarithm of the population within the grid as a function of time at an internuclear separation of $R = 10$. In a non-resonant process we would expect that after the ramp on period this would decay as a straight line of constant slope. However, we see that two separate rates are present. Firstly, there is a large population decrease from 10−15 cycles after which the rate changes to a lower value with a sinusoidal component superimposed. This implies that an intermediate bound state resonance is quickly populated at the start of the pulse after which it begins to decay. The sinusoidal component superimposed is due to Rabi oscillations with the ground state. Such an effect has already been observed in atomic helium through a comparison of the R-matrix Floquet method and the direct solution of the TDSE [26].

4.2 Vibrating nuclei H_2^+ results

In this subsection we present results for vibrating nuclei H_2^+ using a finite difference treatment of the ρ coordinate. Figure 3 presents visualizations of the probability density of vibrating nuclei H_2^+ in the $R - z$ plane for various instants in time during the interaction with the pulse. A grid having extent $-50 \leq z \leq 50$, $0 \leq \rho \leq 42$ and $0 \leq R \leq 26$ Bohr was used. These plots are obtained by integrating the probability density over the ρ coordinate

$$P(z, R, t) = \int \mathrm{d}\rho \; \psi^\star(\rho, z, R, t)\psi(\rho, z, R, t), \qquad (33)$$

and are valuable because they allow us to study the interplay between the dissociation dynamics and the electron dynamics with emphasis on the laser field polarization axis. We only plot that part $-10 \leq z \leq 10$ and $0 \leq R \leq 10$ Bohr since this is the most interesting region. In Figure 3a, near the end of the ramp-on, we see that the electron has clearly responded to the field whereas the nuclear dynamics show no more than a slight distortion. However, later in the pulse as shown by Figures 3b–3d we see nuclear motion occurring with a breakup of the nuclear wavepacket (Fig. 3b) followed by the formation of small *horns* along $z = \pm R$, a signature of dissociative ionization.

4.3 Fixed nuclei H_2 results

Figure 4 displays probability density $P(z_1, z_2, t)$ plotted against (z_1, z_2) at three indicated instants during the exposure of the molecule (with fixed equilibrium spacing $R = 1.4$ Bohr) to soft, intense X-rays ($\lambda = 23$ nm) and 2×10^{16} Wcm^{-2} peak intensity [13]. The most important feature to note (in frame 3 especially) is the tendency for double electron ionization to occur in the $z_1 = -z_2$ quadrants. This indicates at this short wavelength that simultaneous electron ionization involves the two electrons ionizing on opposite sides of the nucleus in contrast to what was found for helium at longer wavelengths.

5 Conclusions

The method that has been presented in this paper represents a general approach for treating accurately and

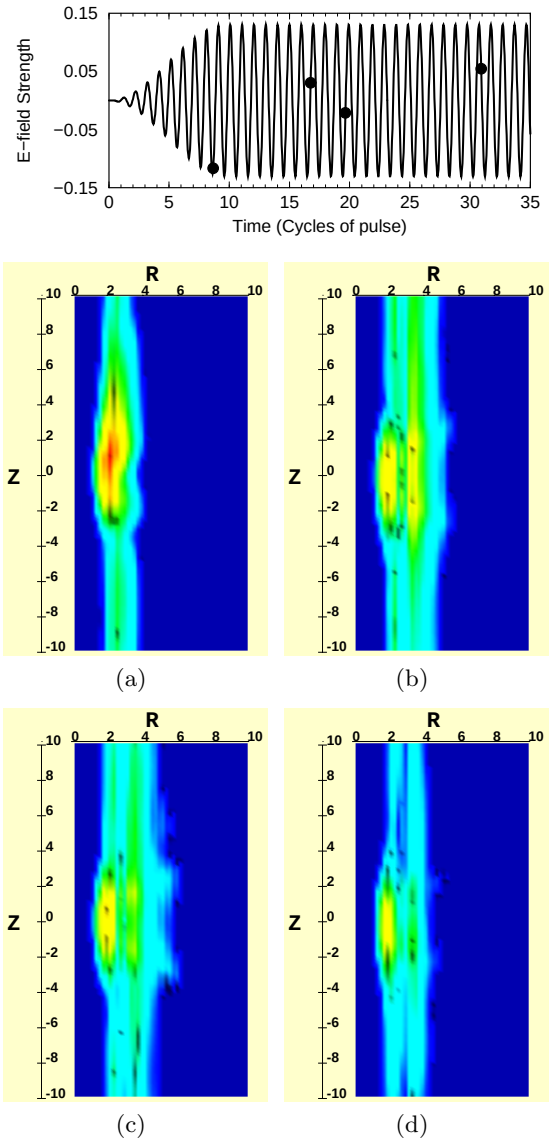

Fig. 3. $R-z$ plots of the electron probability density of vibrating nuclei H_2^+ for a laser pulse having a wavelength of 248 nm and a peak intensity of 6.0×10^{14} Wcm^{-2}. The picture at the top shows a profile of the laser pulse with the circles corresponding (from left to right) to the location of frames (a–d).

reliably few-electron molecules exposed to intense laser pulses. Present day high-end computational resources are essential.

The next extension to this approach will be to include nuclear vibration in the description of H_2. However this problem awaits a Terascale computing facility due to the large increase in memory and computation which will result. For instance the fixed-nuclei H_2 results presented in this paper require roughly 120 Gb of memory. Mapping out the inter-nuclear coordinate would in this case brings the memory requirement up to almost 3 Tbytes.

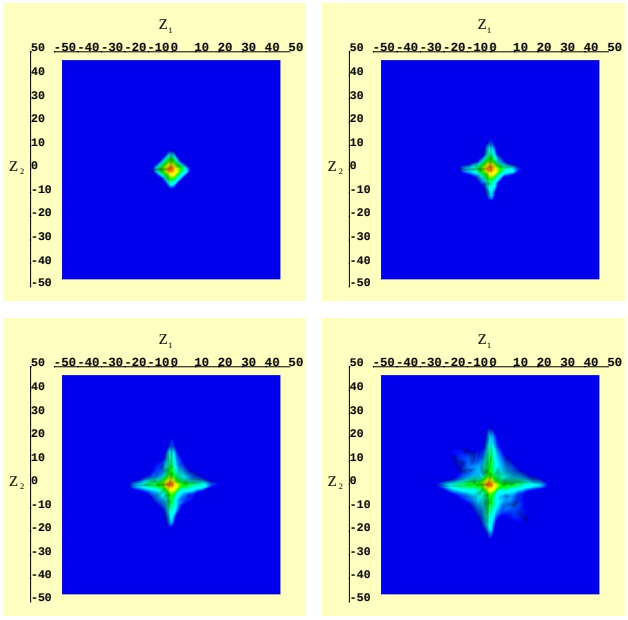

Fig. 4. The dots on the upper E-field plots indicate the instants in time for which the probability density $P(z_1, z_2, t)$ of the hydrogen molecule are portrayed, during its excitation by a 20 field period laser pulse of wavelength 23 nm and of peak intensity 2×10^{16} Wcm^{-2}.

The work reported in this paper is supported in part by the UK Engineering and Physical Sciences Research Council by provision of financial support for DD as well as resources used at the Computer Service for Academic Research, University of Manchester. KJM acknowledges receipt of a studentship award from the Northern Ireland Department of Employment and Learning.

References

1. K. Codling, L.J. Frasinski, J. Phys. B: At. Mol. Opt. Phys. **26**, 783 (1993)
2. A. Giusti-Suzor, F.H. Mies, L.F. DiMauro, E. Charron, B. Yang, J. Phys. B: At. Mol. Opt. Phys. **28**, 309 (1995)
3. J.H. Sanderson, R.V. Thomas, W.A. Bryan, W.R. Newell, A.J. Langley, P.F. Taday, J. Phys. B **31**, L599 (1998)
4. *Molecules & Clusters in Intense Laser Fields*, edited by J. Posthumus (Cambridge University Press, Cambridge, 2001)
5. I.D. Williams, P. McKenna, B. Srigengan, I.M.G. Johnston, W.A. Bryan, J.H. Sanderson, A. El-Zein, T.R.J. Goodworth, W.R. Newell, P.F. Taday, A.J. Langley, J. Phys. B: At. Mol. Opt. Phys. **33**, 2743 (2000)
6. K. Sändig, H. Figger, T.W. Hänsch, Phys. Rev. Lett. **85**, 4876 (2000)
7. M. Plummer, J.F. McCann, L.B. Madsen, Comput. Phys. Commun. **114**, 94 (1998)
8. S. Chelkowski, S. Zuo, A.D. Bandrauk, Phys. Rev. A **46**, R5342 (1992)
9. H. Kono, A. Kita, Y. Ohtsuki, Y. Fujimura, J. Comp. Phys. **130**, 148 (1997)

10. D. Dundas, J.F. McCann, J.S. Parker, K.T. Taylor, J. Phys. B: At. Mol. Opt. Phys. **33**, 3261 (2000)
11. P.G. Burke, J. Colgan, D.H. Glass, K. Higgins, J. Phys. B: At. Mol. Opt. Phys. **33**, 143 (2000)
12. K. Harumiya, I. Kawata, H. Kono, Y. Fujimura, J. Chem. Phys. **113**, 8953 (2000)
13. D. Dundas, K. Meharg, J.F. McCann, K.T. Taylor, in preparation
14. D. Dundas, Phys. Rev. A **65**, 023408 (2002)
15. B. Fornberg, *A practical guide to pseudospectral methods* (Cambridge University Press, Cambridge, 1999)
16. J.C. Light, I.P. Hamilton, J.V. Lill, J. Chem. Phys. **82**, 1400 (1985)
17. M. Hesse, D. Baye, J. Phys. B: At. Mol. Opt. Phys. **32**, 5605 (1999)
18. D. Baye, M. Hesse, J.M. Sparenberg, M. Vincke, J. Phys. B: At. Mol. Opt. Phys. **31**, 3439 (1998)
19. V.S. Melezhik, D. Baye, Phys. Rev. C **59**, 3232 (1999)
20. K. Sakimoto, J. Phys. B: At. Mol. Opt. Phys. **33**, 5165 (2000)
21. D. Baye, P.-H. Heenen, J. Phys. A: Math. Gen. **19**, 2041 (1986)
22. H. Karabulut, E.L. Sibert III, J. Phys. B: At. Mol. Opt. Phys. **30**, L513 (1997)
23. R. Guantes, S.C. Farantos, J. Chem. Phys. **111**, 10827 (1999)
24. R. Guantes, S.C. Farantos, J. Chem. Phys. **113**, 10429 (2000)
25. L.B. Madsen, M. Plummer, J. Phys. B: At. Mol. Opt. Phys. **31**, 87 (1998)
26. J.S. Parker, D.H. Glass, L.R. Moore, E.S. Smyth, K.T. Taylor, P.G. Burke, J. Phys. B: At. Mol. Opt. Phys. **33**, L239 (2000)